Journal of Computational Neuroscience 1, 39–60 (1994).

Intrinsic and Network Rhythmogenesis in a Reduced Traub Model for CA3 Neurons

PAUL F. PINSKY PFPINSKY@HELIX.NIH.GOV
Mathematical Research Branch, NIDDK, National Institutes of Health, Bethesda, MD 20892
Applied Mathematics, University of Maryland, College Park, MD 20742

JOHN RINZEL* RINZEL@HELIX.NIH.GOV
Mathematical Research Branch, NIDDK, National Institutes of Health, Bethesda, MD 20892

Received November 23, 1993; Revised February 24, 1994; Accepted (in revised form) March 17, 1994

Action Editor: R. Traub

Abstract. We have developed a two-compartment, eight-variable model of a CA3 pyramidal cell as a reduction of a complex 19-compartment cable model [Traub et al, 1991]. Our reduced model segregates the fast currents for sodium spiking into a proximal, soma-like, compartment and the slower calcium and calcium-mediated currents into a dendrite-like compartment. In each model periodic bursting gives way to repetitive soma spiking as somatic injected current increases. Steady dendritic stimulation can produce periodic bursting of significantly higher frequency (8–20 Hz) than can steady somatic input (<8 Hz). Bursting in our model occurs only for an intermediate range of electronic coupling conductance. It depends on the segregation of channel types and on the coupling current that flows back-and-forth between compartments. When the soma and dendrite are tightly coupled electrically, our model reduces to a single compartment and does not burst. Network simulations with our model using excitatory AMPA and NMDA synapses (without inhibition) give results similar to those obtained with the complex cable model [Traub et al, 1991; Traub et al, 1992]. Brief stimulation of a single cell in a resting network produces multiple synchronized population bursts, with fast AMPA synapses providing the dominant synchronizing mechanism. The number of bursts increases with the level of maximal NMDA conductance. For high enough maximal NMDA conductance synchronized bursting repeats indefinitely. We find that two factors can cause the cells to desynchronize when AMPA synapses are blocked: heterogeneity of properties amongst cells and intrinsically chaotic burst dynamics. But even when cells are identical, they may synchronize only approximately rather than exactly. Since our model has a limited number of parameters and variables, we have studied its cellular and network dynamics computationally with relative ease and over wide parameter ranges. Thereby, we identify some qualitative features that parallel or are distinguished from those of other neuronal systems; e.g., we discuss how bursting here differs from that in some classical models.

1 Introduction

The CA3 region of the hippocampus generates synchronized epileptiform bursts under a variety of experimental situations in which inhibition has been reduced. Mathematical models (Traub and Miles, 1991, Traub et al., 1991, Traub et al., 1993) of the intrinsic properties of CA3 neurons and their synaptic interactions, in conjunction with experimental slice studies (Chamberlin et al., 1990, Miles et al., 1988, Schwartzkroin and Prince, 1977), have helped elucidate the basic mechanism of bursting in individual cells, and in networks with excitatory synaptic interactions.

Traub et al (1991) recently developed a 19-compartment cable model of a guinea pig CA3 hippocampal pyramidal neuron. Each compart-

*To whom correspondence should be addressed, at MRB, NIDDK, 9190 Wisconsin Ave., Suite 350, Bethesda, MD 20814.

ment contains up to six active ionic conductances that are controlled by ten channel-gating variables. Kinetics for these variables were constructed using somatic voltage clamp data generated by a number of researchers including Kay and Wong (1987), Sah et al (1988a, 1988b), Lancaster and Adams (1986), and Numann et al (1987) from CA3 and other preparations. Conductance densities for each compartment were chosen so as to be consistent with current clamp records from the soma and dendrites of whole neurons, and from isolated apical dendrites (Masukawa and Prince, 1984).

The salient stimulus-response properties of Traub's model neuron include the following. For steady somatic current injection (I_s), weak I_s leads to low frequency (1 Hz) bursting and the frequency increases modestly with I_s (up to about 8 Hz). For intermediate I_s there is aperiodic behavior and for strong I_s periodic spiking occurs. For steady current injection (I_d) at a dendritic location (mid-apical), a larger range of bursting frequencies is attainable (from 1 to 20 Hz). Copies of this neuron model were used to simulate the behavior of a mutually excitatory network with both AMPA (fast relaxing) and NMDA (slowly relaxing) synaptic connections (Traub et al., 1991, 1993). The network model exhibits multiple synchronized population bursts in response to stimulating one cell briefly. The maintenance of synchrony requires a minimal level of AMPA-mediated synaptic coupling, except at very high levels of maximal NMDA conductance. The number of bursts in a finite train can be titrated by increasing the maximal NMDA conductance. At high levels of maximal NMDA conductance synchronized repetitive bursting persists.

We view Traub's CA3 system as a computational analog of an experimental preparation for which all components are known and for which a substantial amount of behavioral repertoire has been described. We ask, what is a minimal biophysical/mathematical description which can account semi-quantitatively for the above (and other) dynamical features of this model system. Just as the Traub model represents the biological CA3 system in an over-simplified but valuable way, we find that this description can be further idealized while still achieving some accountability. Moreover, by reducing the model's complexity and computational demand we seek to identify the dominant qualitative mechanisms for certain aspects of the system's behavior.

Our strategy for reduction is to retain the same active currents and gating kinetics as in Traub's CA3 model but to reduce the number of compartments per neuron to two and the number of currents per compartment. In the Traub model the fast spiking currents (sodium and delayed rectifier) are restricted to the soma and proximal (i.e., within 0.3λ of the soma) dendritic compartments while most (62%) of the calcium channels are located in the distal dendritic compartments. Thus in our model we have segregated the sodium and delayed rectifier currents in a soma-like compartment and the calcium and calcium modulated currents in a dendrite-like compartment. Our reduced model, while tractable enough to permit qualitative analysis, replicates numerous features of the Traub model as described above, including rather complex somatic burst patterns (e.g., Figs. 2 and 3). The simulations described here also serve to illustrate the reproducibility (semi-quantitative) of Traub's computational experiments.

Because our neuron model has relatively few variables and parameters, it requires only modest computational resources, and this enables one to explore rather thoroughly the dependence on parameters. The coupling conductance g_c between our two compartments is a significant electrotonic parameter. We find that bursting can occur only for a range of g_c intermediate between the extremes of small g_c (decoupled compartments) and large g_c (an isopotential cell for which a burst is replaced by a composite sodium-calcium spike). With the prescribed currents, bursting depends on spatiotemporal interactions between the proximal and distal compartments that are possible only with moderate electrotonic coupling. The coupling current reverberates between the two compartments during bursting and prolongs the soma depolarization over that possible with either strong or weak g_c. In this system, a burst is always led by a somatic sodium spike. With moderate coupling, such soma spikes can partially repolarize

thereby drawing current from the dendrite and somewhat delaying the full

dendritic calcium spike; this combination constitutes a burst. This and other features distinguish the bursting found here from that seen in other excitable systems and attributed solely to the combination of ionic currents in an isopotential cell.

Our network model of 100 reduced model cells can also be integrated without computational difficulty. We have studied the effects of different amounts of NMDA and AMPA synapses on population bursting, essentially reproducing some of Traub's numerical results and examining the synchronization phenomena in more detail. saturates and synchronize the cells. As in the Traub network, the synchronization of population activity is not perfect but only approximate. One explanation for this lack of exact synchrony is heterogeneity of cell properties. We show and explain mathematically, however, that even when the cells (and the coupling) are identical, they do not burst precisely together. We also analyze the rapid desynchronization observed following AMPA blockade and demonstrate that it is dependent on heterogeneity in cell properties or on the intrinsic cell trajectories being chaotic.

This is the first in a sequence of our papers on this class of models. Here we present our two-compartment reduction of the Traub model, confirm that it replicates that model's salient features, and explore how the electrotonic coupling parameters effect the model's behavioral properties. In our second paper (Pinsky and Rinzel, 1994) we utilize a phase-plane analysis to gain an intuitive understanding of the mathematical mechanism for repetitive bursting and spiking and to predict the effects of parameter variations on the existence (and frequency) of these solutions. Insights gained from the above analysis allowed us to create an abstract model of an excitatory neural network where each isolated neuron has an intrinsic repetitive "bursting" solution qualitatively similar to that of our two- compartment model. A third paper (Pinsky, 1994) describes this abstract network and presents analytic proofs of some results about burst synchronization.

2 The Model

Figure 1A shows a schematic representation of our model displaying the applied, ionic and synaptic currents for each compartment and the coupling conductance between compartments. The current balance equations for the two compartments are given below:

$$\begin{aligned} C_m V_s' &= -I_{\text{Leak}}(V_s) - I_{\text{Na}}(V_s, h) - I_{\text{K-DR}}(V_s, n) \\ &\quad +(g_c/p)(V_d - V_s) + I_s/p \\ C_m V_d' &= -I_{\text{Leak}}(V_d) - I_{\text{Ca}}(V_d, s) - I_{\text{K-AHP}}(V_d, q) \\ &\quad -I_{\text{K-C}}(V_d, Ca, c) - I_{\text{Syn}}/(1-p) \\ &\quad +(g_c/(1-p))(V_s - V_d) \\ &\quad +I_d/(1-p) \end{aligned} \tag{1}$$

Here V_s, V_d are the deviations of the somatic and dendritic membrane potentials (mV) from a reference potential of -60 mV, I_s (I_d) is the electrode current applied to the soma (dendrite) divided by the total cell membrane area and p is the proportion of cell area taken up by the soma. Ca is the intracellular free calcium level in a sub-membrane "shell" of the dendritic compartment. Because the "effective" shell thickness is indeterminate, there is some arbitrariness in scaling Ca so this quantity is unitless (Traub et al., 1991). Currents and conductances are expressed as densities with units of μA/cm^2 and mS/cm^2, respectively. Capacitance (C_m) is in units μF/cm^2; the time unit is ms.

The kinetic equation for each of the gating variables h, n, s, c and q takes the form

$$y' = (y_\infty(U) - y)/\tau_y(U). \tag{2}$$

The argument U equals V_s when $y = h, n$; V_d when $y = s, c$; and Ca when $y = q$. These equations are supplemented by an equation for Ca handling in the dendritic compartment,

$$Ca' = -0.13 I_{\text{Ca}} - 0.075 Ca \tag{3}$$

We use the same volume/area ratio in our dendrite as does Traub for each dendritic compartment; as in Traub's model, Ca does not diffuse between compartments.

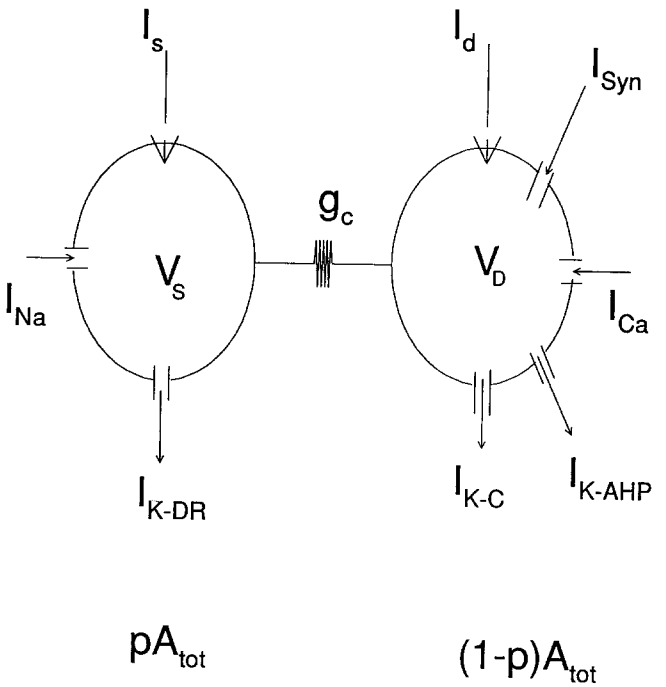

Fig. 1A. Schematic of 2-compartment model showing applied currents and outward and inward active currents to soma and dendrite compartments. Soma has sodium (I_{Na}) and potassium delayed- rectifier (I_{K-DR}) currents; dendrite has calcium (I_{Ca}), Ca activated potassium (I_{K-C}), potassium afterhyperpolarization (I_{K-AHP}) and synaptic (I_{Syn}) currents. Coupling strength between soma and dendrite is governed by parameter g_c. A_{tot} refers to total cell membrane area; in the model it is normalized to 1.

Ionic Currents. The soma-like compartment has two voltage-dependent currents for generating rapid sodium spikes, an inward sodium current I_{Na} and an outward delayed-rectifier potassium current I_{K-DR}. The sodium current activates instantaneously ($m \equiv m_\infty(V_s)$); inactivation, h, of I_{Na} and activation, n, of I_{K-DR} proceed rapidly with time constants of a few milliseconds. Figure 5 illustrates the dependence of frequency on current (f-I relation) for the isolated soma. will As with the Traub model, our soma compartment, as well as the full model, needs a slight hyperpolarizing current for a stable rest state to exist; the rheobase is about $I_s = -0.175$ μA/cm^2 (with $p = 0.5$). The isolated soma shows a wide range of frequencies for maintained I_s from arbitrarily low to a maximal rate around 300 Hz.

The dendritic compartment has three voltage-dependent currents. The inward current I_{Ca} is carried by calcium and its activation, s, is fast. There are two types of potassium currents. The *Ca*-activated potassium current I_{K-C} is proportional to a fast activation variable, c, times a saturating function $\chi(Ca)$. The current I_{K-AHP} has a slow activation variable q which is calcium, instead of voltage, dependent. The time constant for q ranges from 1000 ms at low *Ca* to 100 ms at high *Ca*. The fast activation variables s, c have time constants under 6 *ms* in their effective range. During an active dendritic voltage spike the calcium uptake may be fast, going from near 0 to 300 units in 5 ms; calcium decays with a time constant of 13 ms.

The uncoupled dendritic compartment with no applied current has a stable rest potential of 2 mV. A brief pulse of I_d evokes a single dendritic voltage spike (amplitude 110 mV, 1/2 width 7 ms). Maintained stimulation with small to moderate currents gives rise to very low frequency periodic spiking (Fig. 5).

We summarize the ionic currents below.

$$I_{\text{Leak}}(V_s) = \bar{g}_L(V_s - V_L)$$
$$I_{\text{Leak}}(V_d) = \bar{g}_L(V_d - V_L)$$
$$I_{\text{Na}} = \bar{g}_{\text{Na}} m_\infty^2(V_s) h(V_s - V_{\text{Na}})$$
$$I_{\text{K-DR}} = \bar{g}_{\text{K-DR}} n(V_s - V_{\text{K}})$$
$$I_{\text{Ca}} = \bar{g}_{\text{Ca}} s^2(V_d - V_{\text{Ca}})$$
$$I_{\text{K-C}} = \bar{g}_{\text{K-C}} c\chi(\text{Ca})(V_d - V_{\text{K}})$$
$$I_{\text{K-AHP}} = \bar{g}_{\text{K-AHP}}\, q\, (V_d - V_{\text{K}})$$

Electrotonic Coupling We describe neuronal cable properties with a crudely lumped two-compartment approximation. In compartmental treatments, for which accurate cable behavior is sought, one uses compartments of lengths no greater than about 0.1λ. The sections of Traub's neuron corresponding to our compartments have lengths of 0.5λ or more. Thus our soma and dendrite should be considered as phenomenological compartments. Electrotonic coupling is modeled using the two parameters g_c and p where g_c represents the strength of coupling and p represents the percentage of total area in the soma-like compartment. We do not have an argument for deriving directly values of these lumped cable parameters from the known passive continuous cable parameters of Traub's model.

Suppose we were to proceed naively to get initial estimates. We might imagine the cell, soma and equivalent cylinder dendrite, as a single cable of length l and radius r. Now divide the cable into a proximal (soma-like) compartment and a distal (dendrite- like) compartment of lengths p and $1 - p$ respectively. The core conductance between these two compartments would be $2\pi r^2/(R_i l)$, where R_i is the cytoplasmic specific resistivity (ohm-cm). However, since we scale the currents in each compartment by compartmental area, the coupling conductance g_c for equation (1) would be $g_c = r/(R_i l^2)$. Using the values from Traub et al. (1991) for these constants, we get $g_c \approx 0.18$ mS/cm^2. This value leads to steady state attenuation properties similar to Traub's cable, with attenuation at mid-dendrite in response to subthreshold soma stimulation of about 0.78; however, coupling at this level is too weak to produce bursting.

As described in the Results section, the mechanism for bursting involves a somatic spike initiating an active dendritic voltage spike and thus requires an adequate coupling conductance. This means we need to adjust our estimate to account for attenuation of transients, and in consideration of nonlinear conductances as well. Thus we examine the dependence on g_c of the transient attenuation factor (TAF) in the dendrite in response to a brief square voltage pulse in the soma (Fig. 1B). When the soma's clamped voltage is high, this situation approximates the attenuation of a sodium spike into the dendrite. Attenuation values above 1 indicate an active dendritic voltage spike in response to the square pulse. The figure indicates that g_c values well above 0.18 are needed for an impulse from the soma to cause an active dendritic voltage spike. As $g_c \to \infty$, TAF approaches 1 since the somatic and dendritic voltages are equal at infinite strength coupling. For most simulations here we use $g_c = 2.1$ mS/cm^2. Again we stress that values for our lumped cable parameters, g_c and p, are not yet directly derivable from geometrical and passive electrical neuronal properties. In particular, g_c is not estimated solely as an axial resistance from R_i, r, and l.

Synaptic Interactions. We use the same form for the AMPA and NMDA synapses as used by Traub et al. (1992). AMPA conductance is fast rising and fast decaying while NMDA receptor binding is fast rising but slowly decaying, with a time constant of 150 ms.

The AMPA and NMDA receptors are located in the dendrite compartment.

The NMDA current I_{NMDA} in cell i is given by the expression

$$\bar{g}_{\text{NMDA}} S_i(t)(1 + 0.28\exp(-0.062(V_d - 60)))^{-1} \times (V_d - V_{\text{Syn}})$$

where $\bar{g}_{\text{NMDA}}$ is a parameter measuring absolute NMDA conductance. S_i is determined by the following differential equation:

$$S_i' = \sum_j H(V_{s,j} - 10) - S_i/150 \qquad (4)$$

where $H(x) = 1$ if $x \geq 0$ and 0 otherwise. The sum is taken over all cells j which synapse onto

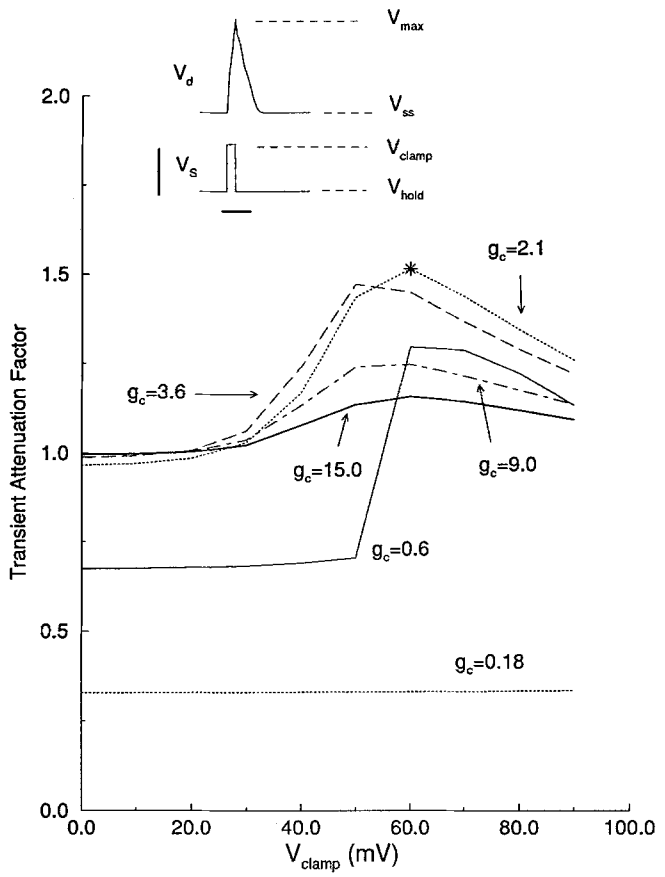

Fig. 1B. Transient attenuation factor (TAF) of voltage from soma to dendrite for different values of g_c. TAF is defined as $(V_{d,\max} - V_{d,ss})/(V_{\text{clamp}} - V_{\text{hold}})$ where $V_{\text{clamp}} - V_{\text{hold}}$ is the magnitude of the square wave voltage clamp applied to the soma (see inset). $V_{d,ss}$ is the steady state dendritic voltage and $V_{d,\max}$ is the maximum dendritic voltage in response to the square wave. Here square wave is of duration 3ms and $V_{\text{hold}} = -10$ mV. TAF is maximal for intermediate values of g_c. Inset shows time courses of V_s and V_d corresponding to $V_{\text{clamp}} = 60$ mV and $g_c = 2.1$ mS/cm^2 (asterisk). Scale bars: 70 mV and 10 ms. and

cell i; $V_{s,j}$ refers to V_s in cell j. As in Traub et al. (1991) we use a saturation parameter $S_{\max}$ which determines the maximum allowable level of $S(t)$; we take $S_{\max} = 125$.

The AMPA current I_{AMPA} is given as $\bar{g}_{\text{AMPA}} W_i(t)(V_d - V_{\text{Syn}})$ where

$$W_i' = \sum_j H(V_{s,j} - 20) - W_i/2 \qquad (5)$$

The term I_{syn} in equation (1) is then the sum of I_{NMDA} and I_{AMPA}.

Because NMDA receptor occupancy decays slowly its value may be nearly constant, at $S_{\max}$, after an initial population burst; note that constancy of S does not mean that NMDA conductance is constant since this latter is voltage dependent. In our single cell analysis we examine the effect of constant NMDA activation (i.e., $S \equiv 125$) as well as the effect of current injection into the soma and dendrite.

All simulations were performed using Fortran on an IBM RS6000 RISC workstation. The differential equations were solved using the classical 4th order Runge Kutta method with a time step of 0.05 ms. Our single neuron model has 8 variables compared to 120 for Traub's; the run time ratio for the two models is 0.09. One second of physiologic time for our 100 cell network took 23 minutes of CPU time.

The functions y_∞ and τ_y and the standard parameter values for the model are listed in the Appendix. At these standard values the system has a stable rest state with $V_s = -4.6$ mV, $V_d = -4.5$ mV (recall V_s and V_d are relative to -60 mV). The corresponding values for the other variables are $h = 0.999$, $n = 0.001$, $s = 0.009$, $c = 0.007$, $q = 0.010$ and Ca = 0.2. These values are initial conditions for all simulations unless stated otherwise.

3 Results

We divide this section into three parts. First we show that our neuron model, with the standard values of the coupling parameters g_c and p, behaves similarly to Traub's model in response to somatic and dendritic stimulation; also in this subsection we analyze a typical burst waveform. Second, we examine in detail the effect of the electrotonic/geometric coupling parameters on our model's behavior; we show that bursting is restricted to a limited range of the (g_c, p) parameter space and that outside this range new behaviors are observed. Finally, we describe the network model and present simulation results which show that our network exhibits the major synchronization properties of Traub's network. We also explore in detail certain aspects of the synchronization process.

3.1 Firing Properties of Two-Compartment Neuron Model Match Those of Traub's CA3 Model

The Traub neuron model exhibits three prototypical repetitive behaviors in response to tonic somatic or dendritic input—periodic somatic spiking, very low frequency bursting and low frequency bursting (Traub et al, 1991). We have found qualitatively similar behaviors in our model under similar input regimes. Here we describe these prototypical behaviors in our model, analyze the burst pattern in detail, and examine the transitions between these behaviors as somatic or dendritic input is increased; in the process, these findings are compared with those of Traub.

Repetitive Firing Patterns. As mentioned in Section 2, both the soma and dendrite compartments (when uncoupled) fire repetitively under constant stimulation, although the dendrite voltage spike is considerably longer in duration (1/2 width 7 ms for V_d and 2 ms for V_s). When electrotonically coupled, these two spike generators give rise to complex spatio-temporal patterns and bursting (burst 1/2 width $\approx$12 ms). Such repetitive, and in fact periodic, bursting can occur for low magnitude current injection to the soma (Fig. 2A) or for steady (dendritic) excitation by NMDA (Fig. 2B). By examining the associated time courses of Ca and q (Fig. 2A,B – right panels) we see that these two slower variables determine the length of the interburst interval. For case A, q is decreasing throughout this interval while Ca decreases to 0 early in the interval and then remains constant. The somatic spike marking the end of the interburst period is triggered when q goes below a threshold value; thus here the time scale of repetitive bursting is determined by the q dynamics. In case B the interburst interval ends when Ca approaches 0. Here q is relatively constant and the sodium spike is triggered by Ca decreasing below a threshold value; thus the time scale is determined by Ca dynamics. In this case, but not in A, the firing pattern would remain essentially the same if we replaced $q(t)$ with its mean value. Traub also found two such qualitatively different repetitive bursting solutions, one whose time scale was dependent on q and one whose time scale was dependent on Ca decay. We denote the first type of bursting, with frequency less than 8 Hz, very-low frequency (VLF) bursting and the second type, with frequency 8–20 Hz, low frequency (LF) bursting.

In both of the above cases the burst is initiated by a sodium action potential in the soma which then triggers a dendritic calcium spike. Below, we examine in detail the burst process. Whether a somatic action potential will trigger a burst, however, depends on the balance between the inward and outward currents in the dendrite. The values of the lumped cable parameters will affect the strength of the coupling current to the dendrite during the somatic action potential; increasing g_c, for example, will increase this

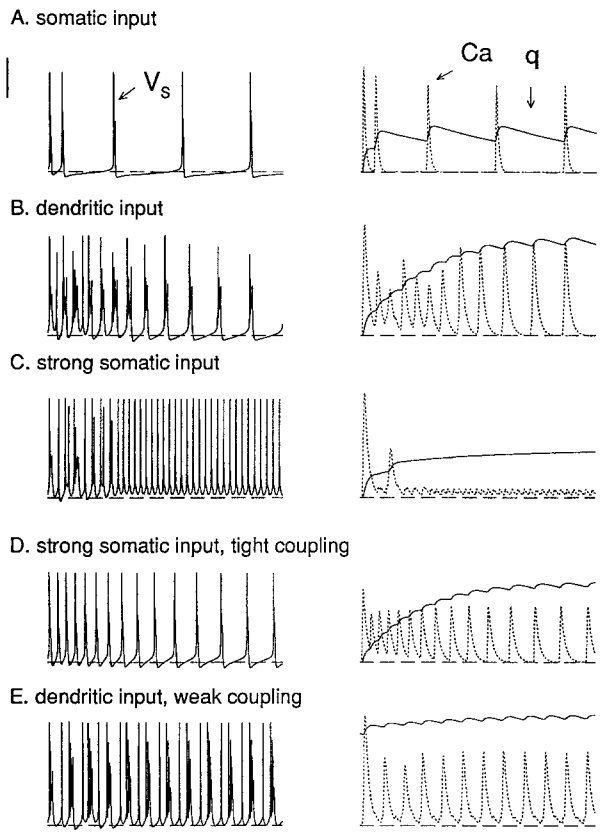

Fig. 2. Variety of firing patterns for different parameter regimes; time courses of somatic voltage, V_s, (left panels), and dendritic variables Ca and q, activation of I_{K-AHP} (right panels). Cases A-E correspond to values of the parameter triple ($I_s(\mu A/cm^2)$, $\bar{g}_{NMDA}(mS/cm^2)$, $g_c(mS/cm^2)$). Very low frequency bursting for somatic current injection in A (0.75, 0.0, 2.1). Steady dendritic synaptic activation in B (−0.5, 1.25, 2.1) causes low frequency bursting. I_s in C (2.5, 0.0, 2.1) is stronger than in A, resulting in high frequency somatic spiking. Conditions of C but with stronger coupling in D (2.5, 0.0, 10.5) leads to soma-dendritic spiking. Weak coupling and dendritic stimulation in E (−0.5, 1.75, 1.425) gives complex periodic orbit: repeating pattern of single spike followed by burst. Standard values of other parameters and standard initial conditions were used in all cases except E where $q(0) = 0.4$. Vertical bar represents 40 mV, 200 Ca units or 0.3 q units; horizontal (time) bar is 200 ms in B–E and 400 ms in A. The horizontal long-dashed lines represent 0 voltage level or 0 Ca (and q) level; the time axis starts at $t = 0$.

current, all other things being equal. Direct stimulation to the dendrite with either I_d or I_{NMDA} will also increase the excitatory drive. The hyperpolarizing currents I_{K-C} and I_{K-AHP} will depend on the levels of q and Ca; these in turn are affected by the stimulation and coupling parameters. Increased levels of q or Ca at the time of the initial somatic action potential will decrease the likelihood that this action potential triggers a dendritic calcium spike.

Generally, high I_s leads to periodic soma spiking without active dendritic spiking as in Fig. 2C where a somatic spike is followed by only a passive response in the dendrite. The hyperpolarizing effect of I_{K-AHP}, as reflected in the high level of q, precludes an active dendritic calcium spike. Here, the q level (when the soma spikes) is greater than that seen in case A where bursting was observed. Although the corresponding q level in B is higher, it is offset by the direct dendritic stimulation present in B but not here. The transient initial burst occurs because of the low initial q value. The passive dendritic response is characterized by minimal calcium conductance and hence minimal increase in Ca and q per sodium spike (see Fig. 2C). The frequency is high (30 Hz) and reflects mainly the dynamics of the soma compartment. A similar high frequency periodic somatic spiking solution characterized by minimal dendritic Ca activity was observed by Traub et al (1993).

Dissection of Burst Waveform. The details of a burst taken from Fig. 2A are displayed in Fig. 3. Qualitatively, this burst is not merely sodium action potentials riding on the longer duration dendritic calcium spike.The electrotonic interaction between soma and dendrite involves significant coupling current that flows back and forth, alternately providing depolarizing or hyperpolarizing current to each compartment. The result is a complex depolarizing event with a duration about twice that of an isolated dendritic spike.

In Fig. 3, we see that the burst sequence is initiated by a somatic sodium spike. This is because I_{Na} is activated at lower voltages than is I_{Ca}. Through electrotonic current spread, this leading sodium action potential depolarizes the dendrite. Then the soma repolarizes, but only

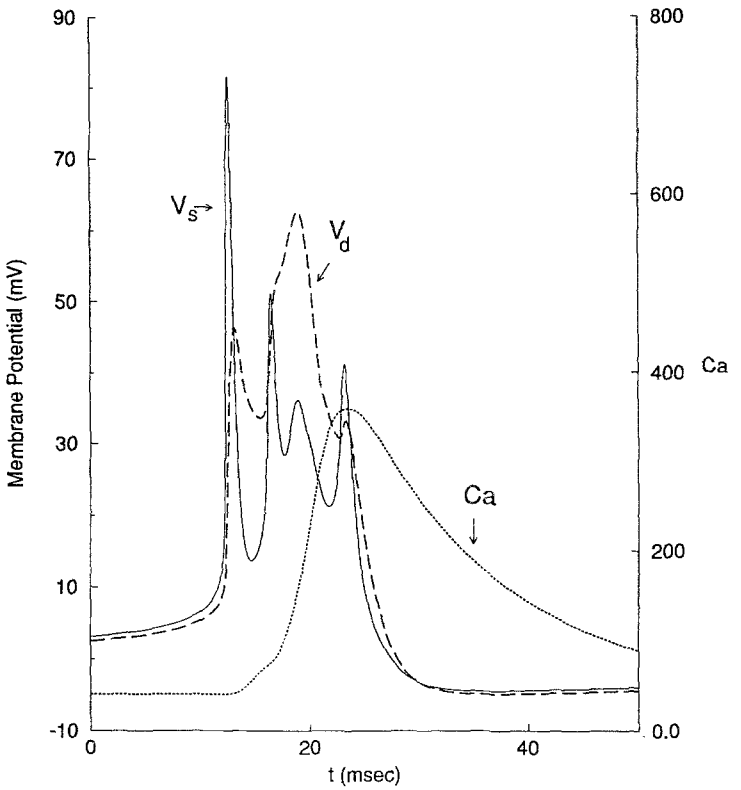

Fig. 3. Time courses of somatic voltage, V_s, dendritic voltage, V_d, and Ca during a burst. Parameters were as in Fig. 2A (note scale for Ca is different than in Fig. 2A). Burst is initiated by somatic action potential which triggers subthreshold dendritic Ca spike. This is followed by full Ca spike in the dendrite leading to somatic burst pattern. Dendritic spike, and hence burst, is terminated by I_{K-C} current which turns on when Ca reaches appreciable levels.

partially. Still it causes V_d to fall somewhat, below the threshold for calcium spike generation, thereby delaying the full dendritic spike. During this repolarization phase, significant coupling current flows into the soma from the dendrite which then initiates a second somatic spike. This second somatic spike stops the drain of coupling current from the dendrite, enabling the dendrite to undergo a full I_{Ca}-mediated voltage spike with accompanying rapid increase in Ca. Note, that the peak of V_d is delayed until about halfway into the burst event. The broad dendritic spike provides an envelope of depolarization which then drives the soma activity. The electrotonic current flowing into the soma is so large, about 40 $\mu A/cm^2$, that the sodium spike generator is over driven. With such strong stimulation the soma would tend, with damped high frequency spiking, toward steady depolarization of 30 mV or more (see below). This behavior is seen here transiently during the regenerative dendritic spike. Some of Traub's (Traub et al., 1991, Figs. 6, 7) simulated bursts show this damped sodium spiking during a burst more clearly. The dendritic calcium spike, and hence the burst, is terminated by I_{K-C}. During V_d's falling phase the coupling current still depolarizes the soma. The current is smaller however, and thereby releases the soma from overdrive, permitting a final partial sodium spike, and an additional slight prolongation to the burst event.

Although I_{K-C} has relatively fast voltage activation, it is also proportional to $\chi(Ca)$. Thus, calcium spike duration is primarily determined by the amount of time required for Ca to build up. The length of the silent phase is determined by the slow variables q and Ca mediating the outward currents I_{K-AHP} and I_{K-C}. For low lev-

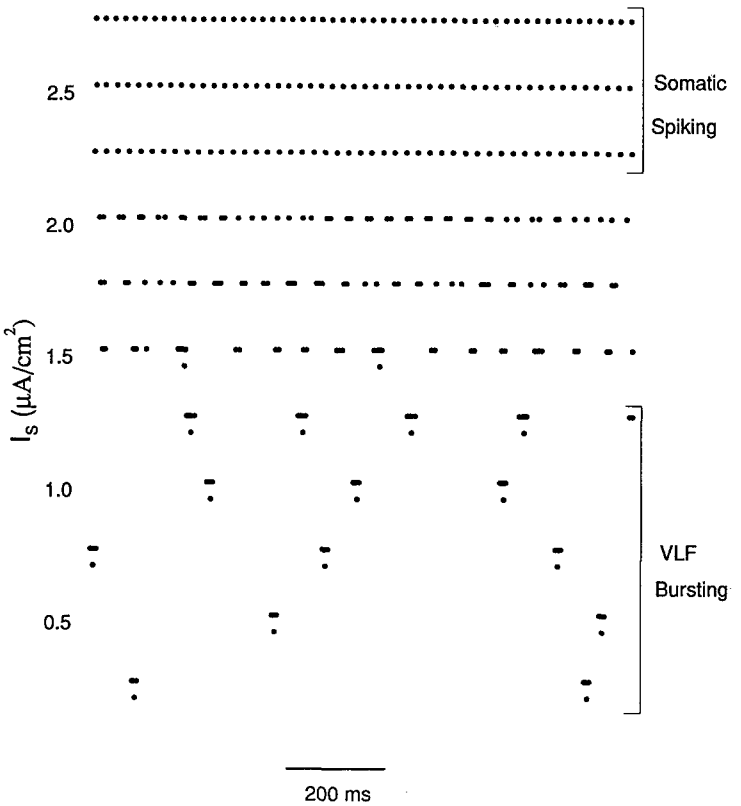

Fig. 4. Soma and dendrite spike trains (raster plots) for steady somatic current injection, I_s. Initial transients have been eliminated. At each I_s level, upper circles represent threshold upcrossings of V_s and lower circles represent threshold upcrossings of Ca. Thresholds were $V_s = 35$ mV, $Ca = 100$. I_s starts at 0.25 μA/cm^2 and increases by 0.25 until a maximum of 2.75 μA/cm^2. Periodic bursting and periodic soma spiking ranges in figure are $0.25 \leq I_s \leq 1.25$ and $2.25 \leq I_s \leq 2.75$ respectively; aperiodic behavior is seen for $1.5 \leq I_s \leq 2.0$.

els of stimulation, both of these currents must decrease before a somatic action potential can be initiated, thus the time scale is that of the slower q (very low frequency bursting). For high stimulus levels, only I_{K-C} need decrease so the time scale is that of Ca decay (low frequency bursting). Of course, the fact that low threshold sodium spiking initiates a burst also contributes to determining burst frequency, making it faster than pure dendritic spiking for, say, a given dendritic input.

This burst mechanism is similar to that seen in Traub's model. A somatic voltage spike initiates the burst, regardless of whether the input is to the soma or the dendrite. Interactions between electrotonically separated sites where either sodium or calcium spiking dominate lead to prolonged soma depolarization.

Response to Steady Somatic Current Injection, I_s. As I_s is increased there is a transition from resting to periodic VLF bursting to somatic spiking (Fig. 4) to steady depolarization. The transitions between bursting and spiking involves aperiodic behavior and regular spiking doublets. These are qualitatively the same transitions observed in the Traub model.

The $f - I_s$ relationship is illustrated in Fig. 5. Here, only the leading spike of a burst is included in the spike count; thus the ordinate represents burst frequency for $I_s \leq 1.25$ and frequency of somatic spiking for $I_s \geq 2.25$ μA/cm^2. Compare with Traub et al. (1991, Fig. 10). The burst frequency increases from 0.3 Hz at $I_s = -0.25$ μA/cm^2 to a maximum of about 4 Hz at $I_s = 1.25$ μA/cm^2. There is roughly an order of magnitude difference between frequen-

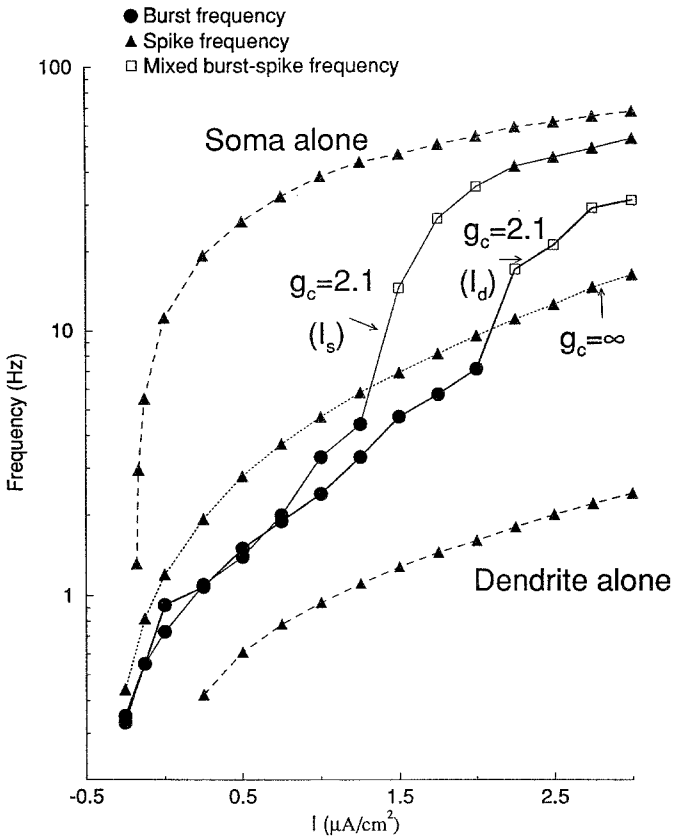

Fig. 5. Frequency current ($f - I$) relation under various coupling regimes. Frequency is determined by the number of times V_s increases past 70 mV (except in the case of the isolated dendrite where we replace V_s with V_d). Dashed curves show $f - I$ for the isolated soma and for the isolated dendrite; here the I on the abscissa indicates I_s and I_d respectively. Solid curves show $f - I$ for standard coupling parameter values (g_c = 2.1 mS/cm^2, p = 0.5) in response to I_s (as in Fig. 4) or I_d. Dotted curve shows $f - I$ for $g_c = \infty$, p = 0.5; here the effect of I_s is equivalent to that of I_d. Circles represent burst frequency while triangles represent spike frequencies (somatic spike frequency for soma alone and for g_c = 2.1, dendritic spike frequency for dendrite alone, and soma-dendritic spike frequency for $g_c = \infty$). Squares correspond to solutions with mixures of bursts and isolated (somatic) spikes; frequency here is combined rate of these events.

cies in the bursting and soma spiking range. In the spiking range the frequency of the full system is somewhat lower than that of the isolated soma due to the current loss to the dendrite. The rheobase however is slightly lower in the full system (I_s = −0.30 μA/cm^2) than in the isolated soma (I_s = −0.175 μA/cm^2) since at rest, or just above, current flows from the dendrite to the soma. Note the negative rheobase indicates that, with no applied current, the neuron undergoes periodic bursting, albeit with very low frequency. For very high I_s (not shown) the amplitude of the somatic spikes diminish until a stable steady state of depolarization (V_s = 33.3 mV) is achieved at I_s = 22.5 μA/cm^2.

We noted above the qualitative similarity between Traub's model neuron and our's with respect to the transition from bursting to spiking with increasing I_s. In fact, we can approximately reproduce the quantitative $f - I_s$ relationship of the Traub model in both the bursting and spiking regimes (Fig. 6). Here in our model we set g_c = 1.85 mS/cm^2 and p = 0.5. To calculate I_s in μA/cm^2 for the Traub model we took the absolute applied somatic current (in μA) given in Traub et al. (1991) and divided by half the neuron model's total area.

Response to Steady Dendritic Input. For increasing dendritic input (current injection or

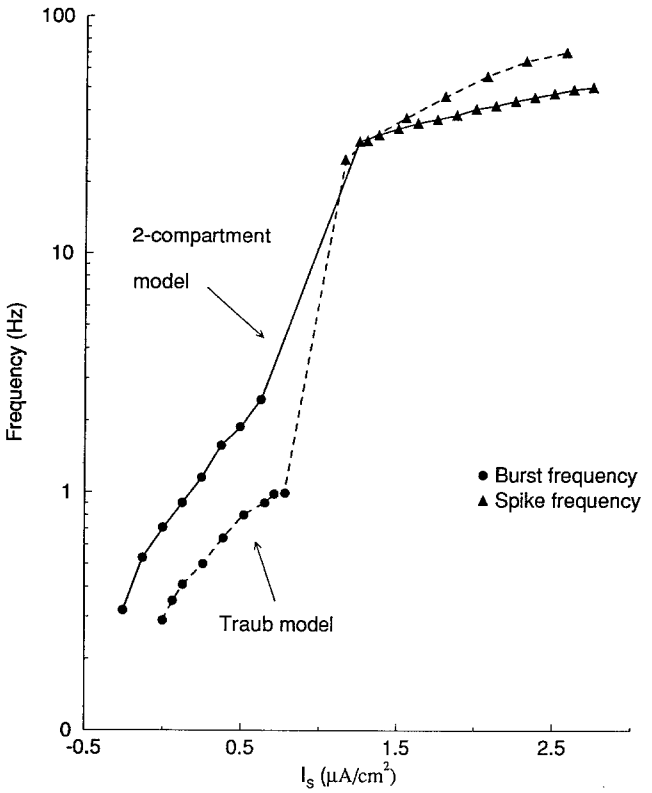

Fig. 6. Frequency versus steady somatic current injection for 2-compartment model (g_c = 1.85 mS/cm^2, p = 0.5) and for Traub model. Burst frequency is indicated with circles and somatic spike frequency with triangles. Both curves show transition from bursting to spiking as I_s is increased. For Traub model, burst and spike frequency data were taken from Traub et al. (1991, Fig. 10); current in μA/cm^2 was determined by dividing absolute current by half the area of the Traub neuron.

synaptic excitation) there is a progression from resting to VLF bursting, to LF bursting (in some cases), to steady depolarization but, with the standard coupling parameter values, no regime of somatic spiking. In the stimulus range for bursting, the frequency of dendritic calcium spikes would decrease if the sodium spike generating currents were blocked because the latter have lower activation thresholds and initiate the calcium spikes associated with bursting.

With $I_s = 0$ the rheobase for I_d is about -0.25 μA/cm^2. As I_d is increased past rheobase we see periodic VLF bursting with frequency increasing up to 7.0 Hz at $I_d = 2.0$ μA/cm^2 (Fig. 5). At about $I_d = 2.25$ μA/cm^2 regular bursting gives way to a chaotic or aperiodic pattern characterized by irregularly spaced bursts with a varying number of spikes per burst. Each burst is associated with a dendritic calcium spike. As seen in Fig. 5, the full system has a higher dendritic spike frequency and lower rheobase than does the dendrite alone due to the higher excitability of the soma. Somatic spiking (with or without dendritic spiking) is not observed for any I_d up to $I_d = 100.0$ μA/cm^2 where a stable rest state is achieved ($V_s = 30.8$ mV, $V_d = 40.9$ mV).

In Fig. 5 the maximum frequency of periodic bursting is about 6 Hz. However, if we give a small hyperpolarizing current to the soma (i.e., $I_s = -0.5$ μA/cm^2), then LF periodic bursting of frequency up to 15 Hz is observed for high I_d. This LF burst pattern is similar to that seen with NMDA excitation in Fig. 2B. VLF bursting is still observed for low I_d and there is a smooth transition between the modes for intermediate I_d; i.e., the burst pattern and regular periodicity remain intact. Thus with a small hyperpolarizing

somatic current the transition with I_d is similar to that seen in the Traub model.

Although not shown here, the firing patterns for increasing $\bar{g}_{\mathrm{NMDA}}S$ progress as those described above. Periodic bursting smoothly changes from VLF to LF as $\bar{g}_{\mathrm{NMDA}}S$ is increased. At higher levels ($\bar{g}_{\mathrm{NMDA}}S \geq 1.75$ mS/cm^2) bursting becomes irregular or chaotic. Periodic somatic spiking was not observed for $\bar{g}_{\mathrm{NMDA}}S$ between 0 and 12.5 mS/cm^2; at this latter value a stable rest state exists with V_s = 33 mV, V_d = 34 mV.

3.2 Dependence of Single Cell Behavior on Electrotonic Parameters

The behaviors and transitions observed were obtained with the standard values of the electrotonic (coupling) parameters. Here we examine in detail the types of firing patterns seen over a large range of coupling parameter values.

When the coupling strength is high, coincident soma-dendritic spiking is usually observed; an example with g_c = 10.5 mS/cm^2 is shown in Fig. 2D. The unitary event of this firing pattern is a composite voltage spike with a high amplitude leading sodium component and a calcium-mediated shoulder. Its duration (7 msec) is that of a dendritic calcium spike and there is appreciable calcium buildup during the dendritic spike. The interburst interval here is similar to that shown in Fig. 2B where the time scale is determined by Ca dynamics. Not shown is another pattern with soma-dendritic spiking where the interburst interval is determined by q dynamics; this is analogous to the situation in Fig. 2A. In either case, the frequency is much higher than if I_{Na} and $I_{\mathrm{K-Dr}}$ were blocked.

Another periodic firing pattern is characterized by one or more isolated somatic spikes preceding a burst (Fig. 2E); this pattern is observed with g_c less than the standard value. This is an example of a complex periodic orbit (see below).

In analyzing behavior for different coupling conditions it is useful to define various categories of firing patterns. Each of the five patterns illustrated in Fig. 2 corresponds to a different one of these categories. A (somatic) burst is a somatic voltage pattern with V_s elevated greater than 10 mV and with at least 3 separate peaks. Periodic bursting is a solution containing a somatic burst followed by a silent phase ($V_s < 5$mV). In periodic dendritic spiking each Ca spike has a maximum of over 100 and is followed by a silent phase where Ca is below 50. Periodic somatic spiking is defined similarly with a maximum V_s of at least 50 and minimum V_s of below 5 mV. Since we have not observed somatic bursting without dendritic spiking, our definition of periodic bursting signifies somatic bursting plus dendritic spiking (as in Figs. 2A,B). When periodic dendritic and somatic spiking coexist we call this soma-dendritic spiking; somatic spiking in the absence of dendritic spiking is denoted as somatic spiking. Restating the definition from Section 3.1, periodic bursting (or soma-dendritic spiking) is very low frequency (VLF) if the rate is less than 8 Hz and low frequency (LF) if the rate is between 8 and 20 Hz. Finally, by complex periodic behavior we mean a periodic orbit which contains more than one depolarized interval; i.e., more than one interval with $V_s > 5$ mV (an example is shown in Fig. 2E).

We now examine the stimulus-response properties of our neuron for different values of coupling strength g_c. Figure 7 summarizes the system's behavior on a two-parameter grid of I_s and g_c. Bursting solutions exist only over an intermediate range of g_c values. For g_c too low (e.g. 1.35 mS/cm^2) only periodic somatic spiking is seen over the range of I_s shown. At high g_c (e.g. 10.5 mS/cm^2 and above) we essentially have a single compartment model. Here only regular VLF or LF soma-dendritic spiking is observed over the range of I_s shown. As shown in Fig. 5, the spike frequency for the effective single compartment is intermediate between that of the isolated soma and that of the isolated dendrite; i.e., the system at g_c = 0.0. The rheobase for the single compartment is lower than that of the isolated soma (or dendrite) however.

For g_c slightly increased from our reference level (e.g., g_c = 3.0 mS/cm^2) we still see VLF periodic bursting over a range of I_s with the threshold for bursting (from steady state behavior) basically unchanged. However, for large I_s, LF periodic bursting is observed instead of somatic spiking. For intermediate I_s (3.75–

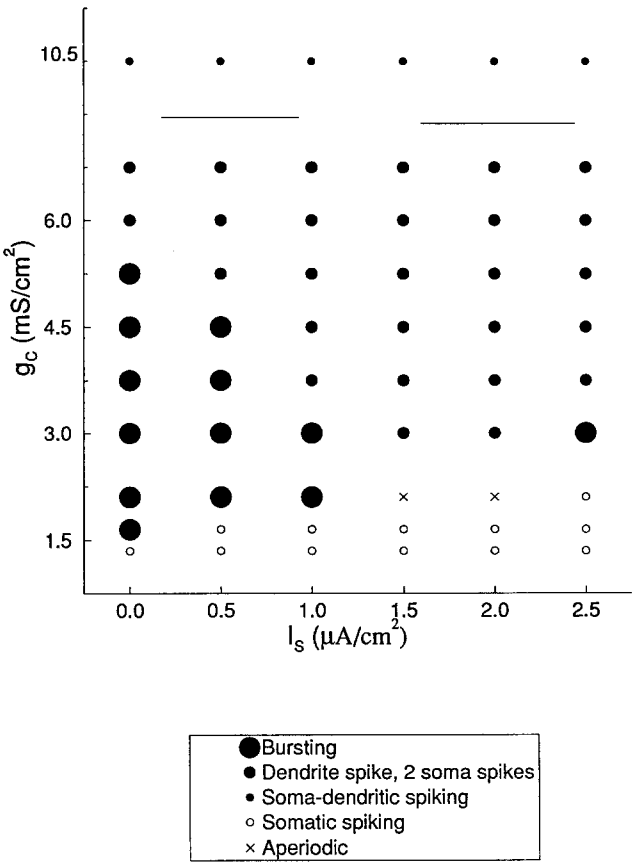

Fig. 7. Firing patterns for a parameter grid of I_s and g_c. At each grid point (I_s, g_c) the type of periodic behavior observed is indicated by the size and shading of the circle; aperiodic behavior is noted by an X. The small, medium and large size circles represent 1, 2 and ≥ 3 somatic spikes respectively per periodic orbit. Filled circles indicate the presence of a dendritic calcium spike. Values of g_c (in mS/cm^2) are 3.0 to 6.75 by .75 plus 1.35, 1.65, 2.1 and 10.5 mS/cm^2; I_s values (in μA/cm^2) are 0.0 to 2.5 by 0.5. At low g_c only somatic spiking is observed while at high g_c only soma-dendritic spiking is seen. At intermediate g_c responses depend on I_s level.

6.75 μA/cm^2) we see VLF to LF dendritic spiking with V_s showing a leading spike followed by a single attenuated spike (not a burst by our arbitrary definition which requires 3 somatic spikes). If we lower g_c from our reference value to 1.65 μA/cm^2 the threshold I_s values for the end of periodic bursting and for the beginning of periodic soma spiking are decreased; the transitions and patterns are similar to those seen in the reference case.

Figure 8 displays the firing patterns for a matrix of $\bar{g}_{\text{NMDA}}S$ and g_c values. As in the case above, bursting is only observed for intermediate g_c values. For very high g_c only soma-dendritic spiking occurs. Pure somatic spiking is observed only for very low g_c. Bursting over most or all of the $\bar{g}_{\text{NMDA}}S$ range is still observed for g_c increased moderately from the reference value. With stronger but limited coupling (i.e., 4.5–7.5 mS/cm^2) burst-like patterns containing only 2 somatic spikes dominate. Aperiodic and complex periodic bursting solutions are usually found in parameter regions that bound the region for bursting. For $\bar{g}_{\text{NMDA}}S$ = 1.5 mS/cm^2 and g_c = 3.0 or 3.75 mS/cm^2, V_s repetitively alternates between a 3-spike and 2-spike burst pattern. The complex periodic bursting solution illustrated in Fig. 2E, a repeating spike-burst pattern, corresponds to $\bar{g}_{\text{NMDA}}S$ = 1.75 mS/cm^2 and g_c = 1.425 mS/cm^2.

We now hold g_c constant at 2.1 mS/cm^2 and and examine how the transition with I_s is af-

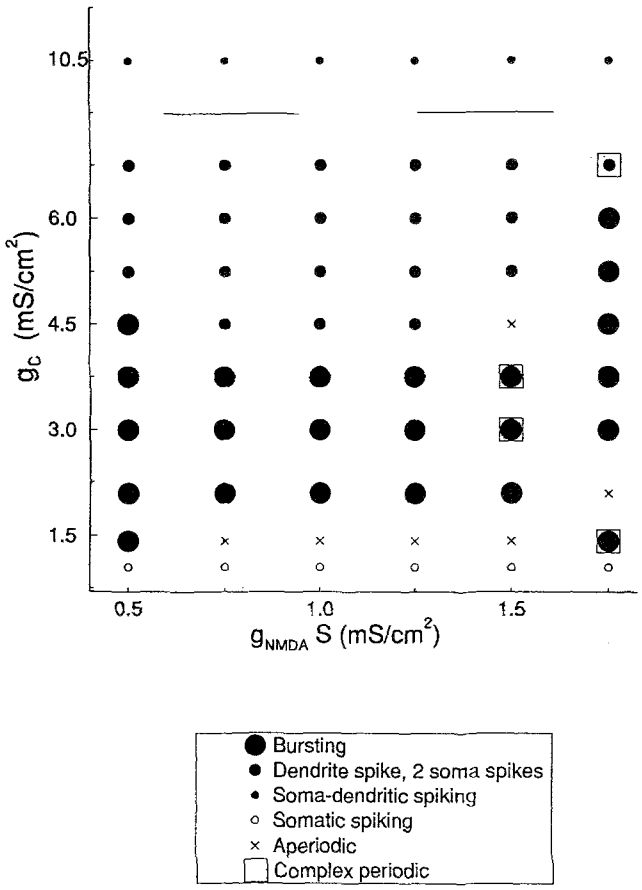

Fig. 8. Firing patterns for a parameter grid of $\bar{g}_{NMDA}$ and g_c. Type of periodic behavior is indicated by the circles as in Fig. 7; the large open square indicates complex periodic behavior. Value of g_c (in mS/cm^2) are 3.0 to 6.75 by 0.75 plus 1.05, 1.425, 2.1 and 10.5 mS/cm^2; S $\bar{g}_{NMDA}$ values (in mS/cm^2) are 0.5 to 1.75 by 0.25. Here I_s was set to -0.5 μA/cm^2. As in Fig. 7, only somatic spiking is observed for low g_c and only soma-dendritic spiking is observed for high g_c. At intermediate g_c levels response depends on magnitude of $\bar{g}_{NMDA}$.

fected by varying p. With $p = 0.25$ or $p = 0.75$ the transition is quite different from the reference case ($p = 0.5$). At $p = 0.25$ the dendritic influence dominates; the whole range of I_s from the steady state threshold to above 2.5 μA/cm^2 (where, with $p = 0.5$, we have periodic soma spiking, cf, Fig. 4) gives rise to periodic VLF bursting. The VLF bursting solution then smoothly changes into an LF bursting solution which persists for an I_s interval of about 0.5 μA/cm^2; for higher I_s complex periodic or aperiodic behavior is observed. For $p = 0.75$ we see rapid soma spiking from $I_s = 0.375$ μA/cm^2 through $I_s = 2.5$ μA/cm^2 and beyond. For very low I_s we see VLF soma-dendritic spiking; bursting is not seen for any I_s when p is so large. The transition between the two modes is seen to be smooth and the maximum calcium levels change only moderately, from 110 to 70 for $I_s = 0.0$ and $I_s = 1.25$ μA/cm^2, respectively.

3.3 Network Behavior

Paralleling Traub et al (1991, 1993), we have formulated an excitatory network of CA3 neurons and have simulated population bursting. We have studied specifically several factors which contribute to the synchronization process, and to the loss of synchrony when AMPA synapses are blocked. Our network simulations were performed with 100 two-compartment model neu-

rons. Since we consider only the disinhibited network, no inhibitory cells are included. Each cell receives NMDA and AMPA synaptic excitation from 20 randomly chosen cells; synaptic weights of a given type are identical for all connections and there are no conduction delays. Hence our network has no spatial structure. When cells are identical the network always has a homogeneous rest or oscillating state, which may or may not be stable (see below). To examine the role of heterogeneity, we introduced for some simulations 10% variation among cells in the parameter $\bar{g}_{Ca}$. With our standard values for intrinsic parameters, the network has a stable rest state at which $S_i = 0$. Our simulated population responses were initiated by inducing a single cell to burst.

The slower NMDA synapses, in particular the level of $\bar{g}_{NMDA}$, primarily determine the network's capacity for sustained bursting. Figure 9 shows synchronized bursting over a range of $\bar{g}_{NMDA}$, with the number of population bursts increasing with $\bar{g}_{NMDA}$ magnitude. For smaller $\bar{g}_{NMDA}$ the population response terminates after a finite number of bursts and the system returns to rest (e.g., panels A, B); for large enough $\bar{g}_{NMDA}$ (panels C, D) synchronized bursting is sustained (here, quasi-periodic). The time course of $S_i(t)$ for a typical cell (dotted) shows a noticeable dip preceding the terminal burst in a finite train response; after this burst, S_i decays to 0 exponentially. In the case of sustained bursting, $S_i(t)$ is nearly constant after the initial population burst.

The simulations in Figs. 9A–C were run with a heterogeneous (10% variability) network. Thus it is not surprising to see some spread in the cell firing times during a population burst, i.e., the network activity time course does not have the square wave shape (all cells firing or no cells firing) characteristic of a perfectly synchronized homogeneous population. Whether or not cells fire precisely together during, what is called, synchronized population bursting depends on a number of factors. Identical cell properties and identical coupling (i.e., a homogeneous network) however do not guarantee perfect synchrony. Rerunning the case of Fig. 9C, but now with a homogeneous network, does not yield perfect synchrony (Fig. 9D). In fact, there is little observable difference between the results in Figs. 9C and 9D, even after many cycles. The mathematical explanation for this is that even though there is a homogeneous bursting solution for the case of Fig. 9D, it is unstable. We observe instead a stable approximately synchronous solution (Pinsky, 1994).

As Traub et al (1993) demonstrated, fast AMPA excitation provides the primary biophysical mechanism for burst synchronization. As shown in Fig. 10A (using parameters values of Fig. 9C), blocking $\bar{g}_{AMPA}$ terminates the synchronized population activity, even though the individual cells continue to burst. In this desynchronized state, $S_i(t)$ in each cell remains nearly constant at $S_{max} = 125$ so $\bar{g}_{NMDA} S \approx 0.014 * 125 = 1.75$ mS/cm^2. Recall in Section 3.1 that the neuron with this constant $\bar{g}_{NMDA} S$ value followed a chaotic trajectory. get We refer to the trajectory with $S_i(t) \equiv S_{max}$ and $\bar{g}_{AMPA} = 0.0$ as the "NMDA-saturated cell trajectory"; note with S_i constant and no AMPA the cells behave as if they are uncoupled.

Two factors contribute to this rapid desynchronization of essentially uncoupled cells. One is heterogeneity in cell properties, and the desynchronization rate generally increases with the degree of heterogeneity. However, in Fig. 10B, where the network is homogeneous, complete desynchronization is still achieved within about 300ms. This highlights the second factor important for desynchronization, namely, the properties of the intrinsic, or in this case, the NMDA-saturated cell trajectories. If these trajectories were periodic and all cells were identical then we would not expect the cells to desynchronize after AMPA was blocked; instead, the phase differences between cells would be constant in time. However, in the present case, a cell's NMDA-saturated orbit is not periodic but chaotic. Chaotic orbits display sensitivity to initial conditions (Reulle, 1989), i.e., trajectories with even small differences in initial conditions rapidly diverge. Thus the small differences in the trajectories of each cell at the time AMPA is first blocked are rapidly amplified, leading to quick desynchronization.

We further tested this idea by doing analo-

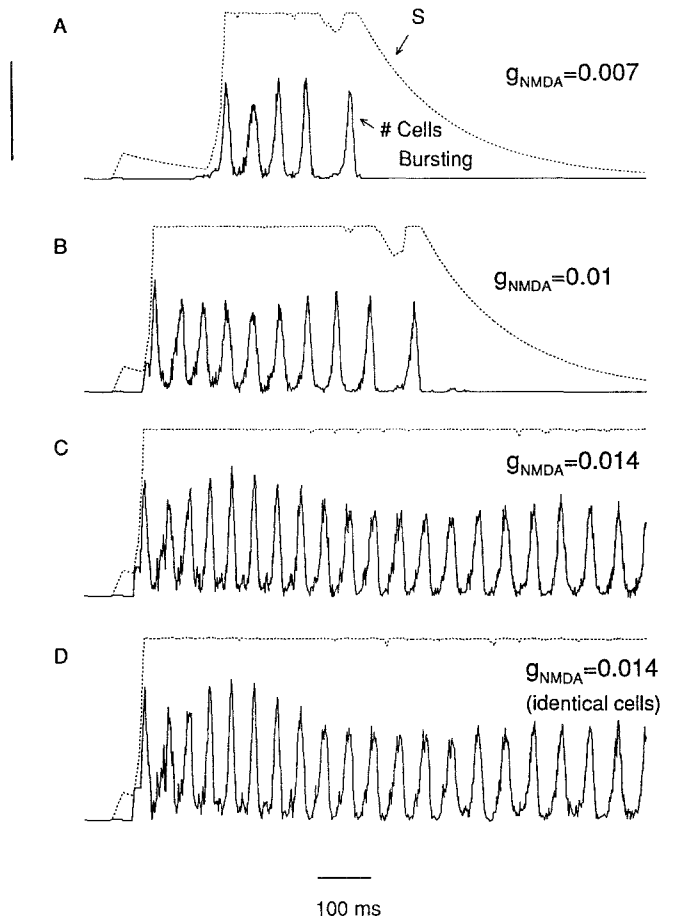

Fig. 9. Population burst patterns for network of 100 cells for different values of $\bar{g}_{NMDA}$. The solid line represents the number of cells with $V_s > 20mV$, denoted as the number of cells bursting. The dotted line is the value of $S(t)$ from a typical cell where $\bar{g}_{NMDA}S(t)$ is the voltage independent part of I_{NMDA}. Vertical bar represents 50 cells or 50 S units. With $\bar{g}_{AMPA}$ fixed at 0.0045 mS/cm^2, the number of population bursts increases with $\bar{g}_{NMDA}$. Past a threshold $\bar{g}_{NMDA}$ level, bursting continues indefinitely. In panels A–C the heterogenous network (10% variation in g_{Ca}) was used while in D we used a homogeneous network, i.e., identical cells. In each case the system was initially at rest when a single cell was stimulated with a brief excitatory input at $t = 0$; I_s was set to -0.5 μA/cm^2.

gous simulations in a different parameter regime where the NMDA-saturated trajectory is strictly periodic. Without variability in cell parameters the network remained partially synchronized when AMPA synapses were blocked (Fig. 10C); with 10% variability in $\bar{g}_{Ca}$ however, the network desynchronized rapidly with AMPA blockade (Fig. 10D).

If $\bar{g}_{AMPA}$ is initially set to 0 then we observe a synchronized primary burst with subsequent loss of synchrony. If $\bar{g}_{NMDA} = 0$ the system exhibits a primary synchronized burst (if $\bar{g}_{AMPA}$ is large enough) with subsequent return to rest. Both of the above properties were also observed in the Traub network.

4 Discussion

Computational modeling offers the opportunity to test hypotheses for how the intrinsic biophysical characteristics of neurons and the coupling properties between cells contribute to the behavior of neuronal ensembles. However, sim-

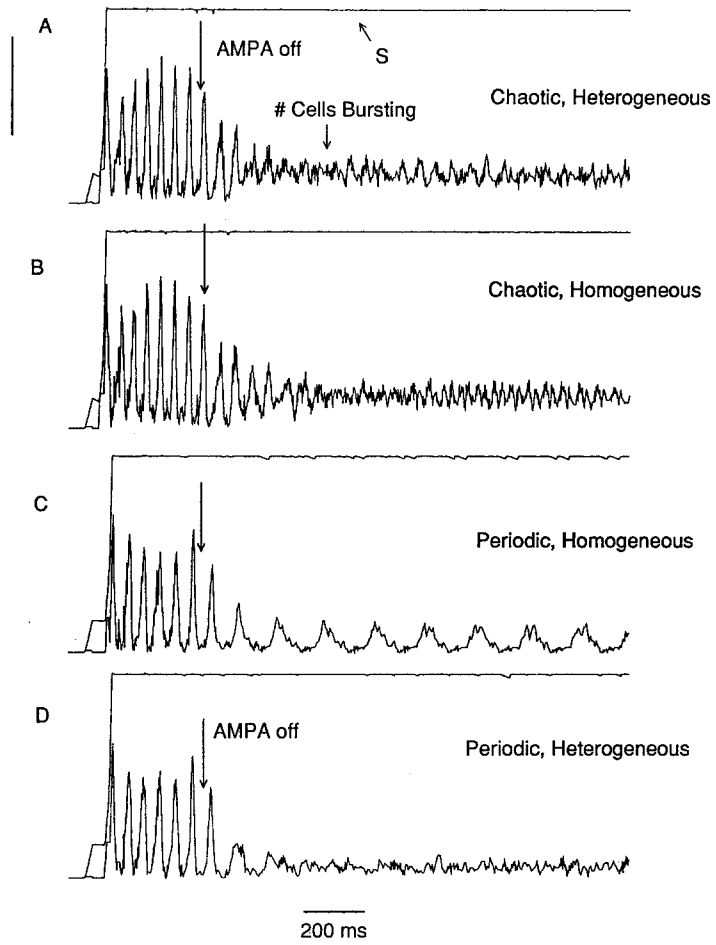

Fig. 10. Desynchronization of population bursting upon AMPA blockade. Line types and axis scalings are as in Fig. 9. In each panel, $\bar{g}_{AMPA}$ is cut off at the arrow. Figures 10A, B show the same simulations as Figs. 9C, D up to the point of AMPA blockade and, as such, correspond respectively to the heterogeneous and the homogeneous network. In 10C, D the network was modified by decreasing the decay rate of S (NMDA receptor occupancy) to 1/1500; $\bar{g}_{NMDA}$ was set to 0.009. Here 10C represents the homogeneous network and 10D represents the heterogeneous network. In 10A, B the "NMDA-saturated" cell trajectories (i.e., with $S_i \equiv S_{Max}$ and $\bar{g}_{AMPA} = 0$) are chaotic while in 10C, D they are periodic.

ulating networks with models that incorporate biophysically realistic elements (dendritic cable properties and different intrinsic ionic currents and synaptic currents with multiple time scales) generally requires considerable computational resources. Moreover, analyzing the model's behavior may require identifying the key parameters and exploring solution dependence over ranges of parameter values. One strives to show trends in behavior for mechanistic interpretation and, occasionally, to reveal the underlying mathematical structure. Inessential details burden the simulations deemed necessary for such in-depth studies. In view of such constraints, some compromises should generally be made about the level of detail to include in a model. Which compromises, depend on the questions under consideration.

An appropriate minimal description contains elements thought to be essential. The pathway to this goal can be from the bottom up (by including additional features when the model is deemed too limited) or from the top down (by hindsightful pruning). The latter may be difficult unless enough parameters are adequately estimated from experimental data *a priori*. In this

paper we have studied a system which is completely specified biophysically. Viewing Traub's computational CA3 network as the given tissue, we have all parameters in hand. Following the bottom-up approach we developed a reduced model, at an intermediate level of detail.

Using the same ionic currents and gating kinetics we reproduce with a two compartment model several major stimulus-response properties of Traub's CA3 neuron model. For example, bursting is found for appropriate ranges of either steady somatic or dendritic stimulation. As I_s increases there is a transition from low frequency bursting to high frequency sodium spiking (without dendritic calcium spikes). For increasing dendritic stimulation the burst frequency rises gradually to higher levels and somatic spiking is not obtainable. The initial event of a burst is a somatic action potential. Then, through a dynamic alternation of potentials and coupling currents between compartments, an active dendritic calcium spike is triggered which produces a depolarization wave upon which somatic spikes ride. Burst frequency depends on stimulus level, but is rate-limited by the two slow recovery processes: the activation variable q for I_{K-AHP} or intracellular calcium which activates I_{K-C}. If either is too high at the time of the initial somatic spike an active dendritic calcium spike is precluded. One or the other of these slow processes (in different parameter regimes) can determine the interburst interval.

Bursting in these CA3 models depends on having the lower threshold, fast, sodium spike-generating currents and the higher threshold, slower Ca and Ca-dependent currents in electrically separated compartments and on the dynamic electrotonic current flows between these compartments. No single compartment in Traub's neuron model, or in ours, can burst if isolated. Increasing the strength of coupling between soma and dendrite so that there is essentially a single compartment abolishes bursting in our model (Fig. 5) and leads to a combined sodium-calcium spike. Figure 5 summarizes well several of these points. An isolated soma spikes at relatively high sustained rates, while an isolated dendrite fires calcium spikes only at low rates. Very strong coupling yields frequencies between those of the isolated compartments, but does not allow bursting. With intermediate coupling the model shows two modes of behavior, low frequency bursting and rapid sodium spiking, in different stimulus regimes. For either response mode the model's firing frequency lies between the frequencies of the correspondingly stimulated uncoupled compartments. Calcium spiking in a stimulated dendrite is accelerated by sodium spikes originating in a soma compartment. Conversely, Ca-mediated dendritic K^+ currents slow the rate of pure somatic spiking. Because of our model's modest computational overhead we could characterize thoroughly by simulation the properties of bursting and other response patterns and the ranges of coupling strength where they occur. With ease, we could match semi-quantitatively the frequency-current relation of our model with Traub's (Fig. 6).

Llinas (1975) was among the first to convincingly demonstrate the spike generating ability of dendrites. Wong et al (1979) showed that slow Ca spikes, as well as fast Na spikes, were produced in the dendrites of CA3 pyramidal cells. Nonuniformity of channel densities, along with spike generating ability in the dendrites, has since been recognized and simulated as a mechanism for bursting in other CNS cells (Rhodes and Gray, 1993, Upinder and Bower, 1993, Kim and Connors, 1993). In these cases, as here, the reverberating electrotonic current between the soma, dense in sodium channels, and the dendritic regions, which have most of the calcium channels, leads to complex dynamic spike patterning. This mechanism may be contrasted with those involving fast and slow processes in isopotential neuron models, such as the *Aplysia* R-15 parabolic burster (e.g., Rinzel and Lee, 1987) or the thalamic relay neuron (e.g., Rush and Rinzel, 1993). In these latter cases, blocking the Na^+ current leaves an underlying slow wave with essentially the same frequency as repetitive bursting. In our case, blocking sodium spikes generally lowers the slow wave frequency considerably, and may eliminate calcium spiking.

Another distinguishing feature of this bursting type is that the transition to continuous spiking activity does not appear to involve a gradual lengthening of the burst's spiking phase,

as happens in many single-compartment burst mechanisms. Rather, we see in the transition regime rather complex time courses of sequences of bursts and spikes, but not with long duration bursts. As the stimulus intensity increases the number of bursts decreases until we see only somatic spiking. Finally, in many known burst mechanisms the spike frequency just beyond the transition into continuous spiking is comparable to that seen within the burst. Here, the continuous sodium spike rate is much lower than that during a burst's calcium spike. As noted in Section 3.1, this is because the dendritic spike transiently supplies a strong depolarizing current to the soma which drives it to fire at very high rates.

Our observation that the leading somatic sodium spikes of a burst have a considerable enhancing effect on burst frequency suggests an experiment (computational for Traub's model, or biological for hippocampal or cortical slice) for neurons that exhibit such bursting. We would predict that for dendritic input (e.g, steady glutamate to activate NMDA synapses) the response frequency would drop significantly if sodium spikes were blocked. We have found with our model however that it is important to eliminate both I_{Na} and I_{K-DR}. Blocking only I_{Na} precludes repetitive calcium spiking for dendritic input. Since I_{K-DR} is present in half of our model neuron's membrane, it provides a substantial hyperpolarizing effect that is not easily overcome with our coupling parameters set to their standard values.

Our model is minimal in that bursting is achieved with only two compartments and with complete segregation of the two classes of currents. Although combining the currents in a single compartment (large g_c) precludes bursting *per se* each Na spike becomes the leading edge of a prolonged Ca-mediated depolarization. This could indeed lead to multiple axon spikes downstream and perhaps still drive network oscillations. On the other hand, this sodium-calcium spike is briefer than the depolarization of a burst mediated by the changing sign of the coupling current. Moreover, this further reduction to a single-compartment neuron eliminates only one variable and disallows the exploration of electrotonic effects.

As noted previously, if currents were not segregated by intermediate coupling conductance the neuron model could not switch firing modes from bursting to pure somatic spiking in response to a changing I_s. Mode switching could also be realized by adjusting the coupling conductance. For example, bursting could give way to continuous spiking if the distal compartment became more remote. A physiological mechanism could involve modulators that might, for instance, change a potassium leakage conductance and make the membrane more leaky, effectively decreasing λ. In our idealized model neuron, the simplest analog would be a decrease in the phenomenological coupling g_c.

The existence of bursting also requires an adequate relative size $(1-p)$ of the dendrite-like compartment. Our analysis showed that if it is too small, say $(1-p) < 0.25$, the cell did not exhibit bursting, only fast spiking. This suggests that if we decrease $\bar{g}_{Ca}$ (with $p = 0.5$) we would also get a transition from bursting to spiking (at an appropriate level of I_s). Computed results (not shown here) indicate that (with $I_s = 0.5$) bursting is observed for $\bar{g}_{Ca}$ (mS/cm^2) from 10.0 through 8.0 and somatic spiking is observed for $\bar{g}_{Ca}$ below 7.0; in between we see aperiodic behavior. Traub et al. (1993) found that decreasing $\bar{g}_{Ca}$ by 50% in his network model leads to a high frequency series of action potentials in all cells.

Our model has several time scales for intrinsic recovery processes. The time constant of q is between 100 and 1000 ms while the other gating variables all have time constants of less than 6 ms (in their effective range). Ca decays with an intermediate time constant (13 ms) while it increases rapidly in the presence of I_{Ca}. We have developed a phase-plane approach for analyzing this model which exploits these different time scales (Pinsky and Rinzel, 1994). Because Ca may increase rapidly, the standard approach of considering the averaged vector field of (q, Ca) must be modified. Our analysis has led to discoveries of new model behaviors; for instance, we saw that increasing the Ca removal rate can

lead to bistability with coexistence of stable LF bursting and somatic spiking.

Our CA3 network, even when homogeneous, rapidly desynchronizes when AMPA is blocked. We showed that this relates to the fact that the NMDA-saturated cell trajectories are chaotic. Hansel and Sompolinsky (1992) found that in large networks chaotic behavior can underlie rapid desynchronization while noise (in the absence of chaos) is a relatively slow and inefficient desynchronization mechanism; their findings are related to the binding problem in the visual cortex. These examples demonstrate that the presence of chaos may have important physiologic consequences.

Our minimal model provides a framework for exploring some general aspects of electrotonic segregation of channel types in neurons and of coupling interactions in excitatory networks, and it is suitable for analysis and parameter variation studies. Insights derived from this model have helped us derive an abstract model of an excitatory network for which we can prove some results on synchronization (Pinsky, 1994). Analysis of this abstract model has led to the prediction that "approximately synchronous" solutions may exist even when the homogeneous solution is unstable, precisely the situation described above in our network results.

Acknowledgments

We thank Roger Traub, Mike Gutnick, Idan Segev and the referees for helpful comments.

Appendix

We list the functions α_y, β_y below where $y_\infty = \alpha_y/(\alpha_y + \beta_y)$ and $\tau_y = 1/(\alpha_y + \beta_y)$.

$$\alpha_m = \frac{0.32(13.1 - V_s)}{\exp((13.1 - V_s)/4) - 1)}$$

$$\beta_m = \frac{0.28(V_s - 40.1)}{\exp((V_s - 40.1)/5) - 1)}$$

$$\alpha_n = \frac{0.016(35.1 - V_s)}{\exp((35.1 - V_s)/5)) - 1}$$

$$\beta_n = .25\exp(.5 - .025V_s)$$

$$\alpha_h = 0.128\exp((17 - V_s)/18)$$

$$\beta_h = \frac{4}{1 + \exp((40 - V_s)/5))}$$

$$\alpha_s = \frac{1.6}{1 + \exp(-0.072(V_d - 65))}$$

$$\beta_s = \frac{.02(V_d - 51.1)}{\exp((V_d - 51.1)/5)) - 1}$$

$$\alpha_c = \frac{\exp((V_d - 10)/11) - \exp((V_d - 6.5)/27)}{18.975}$$

for $V_d \leq 50$

$$\alpha_c = 2.\exp((6.5 - V_d)/27) \text{ for } V_d > 50$$

$$\beta_c = 2.\exp((6.5 - V_d)/27) - \alpha_c$$

for $V_d \leq 50$

$$\beta_c = 0 \text{ for } V_d > 50$$

$$\alpha_q = \min((0.00002)Ca, 0.01)$$

$$\beta_q = 0.001 \qquad (6)$$

The standard values of the parameters are given below. The maximal conductances (in mS/cm^2) are $\bar{g}_L = 0.1$, $\bar{g}_{Na} = 30$, $\bar{g}_{K-DR} = 15$, $\bar{g}_{Ca} = 10$, $\bar{g}_{K-AHP} = 0.8$, $\bar{g}_{K-C} = 15$, $\bar{g}_{NMDA} = 0.0$ and $\bar{g}_{AMPA} = 0.0$. The reversal potentials (in mV) are $V_{Na} = 120$, $V_{Ca} = 140$, $V_K = -15$, $V_L = 0$ and $V_{Syn} = 60$. The applied currents (in $\mu A/cm^2$) are $I_s = -0.5$ and $I_d = 0.0$. The coupling parameters are $g_c = 2.1 mS/cm^2$ and $p = 0.5$. The capacitance, C_M, is $3\mu F/cm^2$ and $\chi(Ca) = \min(Ca/250, 1)$. Values for these parameters, and these function definitions, are taken from Traub et al, 1991.

References

Chamberlin, N., Traub, R., and Dingledine, R. (1990). Spontaneous EPSPs initiate burst-firing in rat hippocampal neurons bathed in high potassium. J. Neurophysiol. 64:1000–1008.

Hansel, D. and Sompolinsky, H. (1992). Synchronization and computation in a chaotic neural network. Phys. Rev. Lett. 68:718–721.

Kay, A. and Wong, R. (1987). Calcium current activation kinetics in isolated pyramidal neurons of the CA1 region of the mature guinea-pig hippocampus. J. Physiol. Lond. 392:603–616.

Kim, H. and Connors, B. (1993). Apical dendrites of the neocortex: correlation between sodium- and calcium-dependent spiking and pyramidal cell morphology. J. Neurosci. 13:5301–5311.

Lancaster, B. and Adams, P. (1986). Calcium dependent cur-

rent generating the afterhyperpolarization of hippocampal neurons. J. Neurophysiol. 55:1268–1282.

Llinas, R. (1975). Electroresponsive properties of dendrites in central neurons. In: Kreutzberg, G., ed. Advances in Neurobiology, Vol 12. Raven Press, New York. pp. 1–12.

Masukawa, L. and Prince, D. (1984). Synaptic control of excitability in isolated dendrites of hippocampal neurons. J. Neurosci. 4:217–227.

Miles, R., Traub, R., and Wong, R. (1988). Spread of synchronous firing in longitudinal slices from the CA3 region of the hippocampus. J. Neurophysiol. 60:1481–1496.

Numann, R., Wadman, W., and Wong, R. (1987). Outward currents of single hippocampal cells obtained from the adult guinea pig. J. Physiol. Lond. 393:331–353.

Pinsky, P. and Rinzel, J. (1994). Phase-plane analysis of a reduced Traub model of a CA3 pyramidal neuron. In preparation.

Pinsky, P. (1994). Synchrony and clustering in an excitatory neural network with intrinsic relaxation kinetics. Siam J. Appl. Math. (in Press).

Rhodes, P. and Gray, C. (1993). Simulations of intrinsically bursting neocortical pyramidal neurons. Neural Computation (in Press).

Rinzel, J. and Lee, Y. (1987). Dissection of a model for neuronal parabolic bursting. J. Math. Biol. 25: 653–675.

Ruelle, D. (1989). Elements of Differentiable Dynamics and Bifurcation Theory. Academic Press, San Diego, Ca.

Rush, M. and Rinzel, J. (1993). Analysis of bursting in a thalamic neuron model. Biol. Cybern. (in Press).

Sah, P., Gibb, A., and Gage, P. (1988a). The sodium current underlying action potentials in guinea pig hippocampal CA1 neurons. J. Gen. Physiol. 91:373–398.

Sah, P., Gibb, A., and Gage, P. (1988b). Potassium current activated by depolarization of dissociated neurons from adult guinea pig hippocampus. J. Gen. Physiol. 92:263–278.

Schwartzkroin, P. and Prince, D. (1977). Penicillin-induced epileptiform activity in the hippocampal in vitro preparation. Annals of Neurology 1:463–469.

Traub, R. and Miles, R. (1991). Neuronal networks of the hippocampus. Cambridge University Press, New York.

Traub, R., Wong, R., Miles, R., and Michelson, H. (1991). A model of a CA3 hippocampal pyramidal neuron incorporating voltage-clamp data on intrinsic conductances. J. Neurophysiol. 66:635–649.

Traub, R., Miles, R., and Buzsaki, G. (1992). Computer simulation of carbachol-driven rhythmic population oscillations in the CA3 region of the in vitro rat hippocampus. J. Physiol. Lond. 451:653–672.

Traub, R., Miles, R., and Jefferys, J. (1993). Synaptic and intrinsic conductances shape Picrotoxin-induced synchronized afterdischarges in the guinea-pig hippocampal slice. J. Physiol. Lond. 93:525–547

Upinder, B. and Bower, J. (1993). Exploring parameter space in detailed single neuron models: simulations of the mitral and granule cells of the olfactory bulb. J. Neurophysiol. 69:1948–1965.

Wong, R., Prince, D., and Basbaum, A. (1979). Intradendritic recordings from hippocampal neurons. Proc. Natl. Acad. Sci. 76:986–990.